Seismic fragility analysis of masonry structures considering the effect of mainshock-aftershock sequences

Zhang, Yongqun; Wang, Zhuolin; Jiang, Lixue; Skalomenos, Konstantinos; Zhang, Dongbo

DOI:
10.1016/j.engstruct.2022.115287

Document Version
Peer reviewed version

Citation for published version (Harvard):
Zhang, Y, Wang, Z, Jiang, L, Skalomenos, K & Zhang, D 2023, 'Seismic fragility analysis of masonry structures considering the effect of mainshock-aftershock sequences', *Engineering Structures*, vol. 275, 115287. https://doi.org/10.1016/j.engstruct.2022.115287

Seismic fragility analysis of masonry structures considering the effect of mainshock-aftershock sequences

Yongqun Zhang[a,b,c], Zhuolin Wang[c*], Lixue Jiang[c], Konstantinos Skalomenos[d], Dongbo Zhang[c]

a. Key Laboratory of Earthquake Engineering and Engineering Vibration, Institute of Engineering Mechanics, China Earthquake Administration, Harbin, China

b. Key Laboratory of Earthquake Disaster Mitigation, Ministry of Emergency Management, Harbin, China

c. Shanghai Key Laboratory of Engineering Structure Safety, Shanghai Research Institute of Building Sciences Co. Ltd, Shanghai, PR China

d. Department of Civil Engineering, The University of Birmingham, B15 2TT, Edgbaston, Birmingham, United Kingdom

Abstract: Earthquake investigations indicate that strong aftershocks can further aggravate the structural damage and low attention has been given to understand the seismic performance of masonry structures under seismic sequences. This manuscript studies the seismic fragility of masonry structures considering the effect of aftershocks by proposing a simplified probabilistic approach. In total, 36,000,000 stochastic earthquake-structure samples were generated using Monte Carlo simulation to consider the uncertainty of earthquake ground motions and structures, while seismic fragility curves of masonry structures were obtained by considering the following parameters:

1) aftershock intensity, 2) seismic wall area ratio, 3) site conditions, 4) the number of storeys, 5) reinforced concrete (RC) tie column, 6) mortar strength. The interstorey drift ratio was employed to assess the structural performance levels. The results showed that strong aftershocks have a significant influence on the fragility curves of masonry structures. The probability of exceeding the collapse limit state of structures can increase by 32.2% due to aftershock effect. Among the examined parameters it was found that the number of storeys has the greatest effect on the seismic fragility of masonry structures. By increasing the number of storeys, the probability of exceedance of the collapse damage state can increase up to 28.7%. The derived fragility curves are validated against a finite element method, which indicate the rationality of the proposed methodology.

Key words: masonry structures; mainshock-aftershock sequences; fragility curves; seismic performance assessment; uncertainty

1 Introduction

Past earthquakes showed that a major earthquake (mainshock) is always followed by secondary earthquakes (aftershock), and the mainshock and the aftershocks constitute a mainshock-aftershock (M-A) sequence. Although the magnitude of aftershock tends to be lower than that of the mainshock, the aftershock can still produce moderate and strong ground motions that can further aggravate the structural damage produced by the mainshock. The aftershock events of the 1999 Chi-Chi earthquake [1], the 2008 Wenchuan earthquake [2], the 2010 New Zealand earthquake [3], the 2011 Tohoku earthquake [4], and the 2015 Nepal earthquake [5] further increased structural damage of structures caused by the main event and in some cases led to the structural collapse, resulting in an increase in casualties and economic losses. Meanwhile, it has been observed that no effective repair or strengthening works can be done within short interval between a mainshock and the corresponding aftershock [6]. To investigate the effect of aftershocks, several researchers have studied the effect of M-A sequences on structures, mainly on reinforced concrete frames [7][8][9][10], steel frames [11][12][13], and wooden structures [14][15]. However, less attention has been paid to masonry structures [16], and the related fields still need to be further studied.

Masonry structures have been widely used in China due to its simple construction and low cost. However, masonry structures exhibit obvious brittle characteristics and poor structural integrity due to the low tensile, flexural and shear strength of masonry. As a result, masonry structures are seriously damaged by earthquakes [17], especially, under M-A sequences. Vulnerability assessment is a commonly used method to evaluate structural performance. Sun and Zhang [18] proposed seismic damage probability matrices based on 38 regions in 17 earthquake events. Asteris et al. [19] conducted a vulnerability assessment method of historical masonry structures by utilizing a finite element method. Borzi et al. [20] and Ahmad et al. [21] established a simplified pushover-based method for masonry structures to obtain the fragility curves. Lagomarsino et al. [22] proposed a macroseismic vulnerability model for existing masonry buildings, which can be used for seismic risk assessment on a regional and national scale. Shabani et al. [23] reviewed the simplified analytical methods for the seismic vulnerability assessment of unreinforced masonry structures. To consider the effect of aftershocks, Rinaldin and Amadio [16] studied the structural response through time history dynamic analysis on a single-degree-of-freedom (SDOF) system. It has been seen from the above studies that although fragility analysis is a well-accepted method to analyze the seismic vulnerability of masonry structures, the effect of aftershocks is ignored.

This manuscript tends to propose a simplified probabilistic approach for seismic fragility of masonry structures. According to the location of RC tie columns of masonry structures built in different times, the masonry structures are divided into five categories, and the corresponding performance levels and interstorey drift ratio thresholds for assessing their seismic performance are defined. In total, 36,000,000 stochastic earthquake-structure system models are developed to support the construction of the M-A fragility curves of masonry structures. The effects of the seismic wall area ratio, aftershock intensity, site condition, number of storeys, RC tie column, and mortar strength are systematically investigated.

2 Seismic vulnerability assessment

Fragility curves are often used to describe the conditional probability that a structure can reach or exceed for a given damage state resulted by subjecting the structure to a ground motion with a specific intensity. To obtain the seismic fragility curves of building structures, the peak ground acceleration (PGA) of ground motions is used as the intensity of input ground motions according to the current seismic design codes [24]. Considering the lognormal distribution assumption of structural response and damage limit state, the conditional probability P(·) that the interstorey drift ratio demand of structures $IDR_{\max}|\mathrm{PGA}$ exceeds the interstorey drift ratio capacity of damage limit state for a given PGA can be calculated from Eq.(1).

$$P\left(IDR_{\max}\left|PGA > IDR_{LSi}\right.\right) = 1 - \Phi\left(\frac{\ln\left(IDR_{LSi}/\overline{IDR}_{\max}\right)}{\sqrt{\beta_c^2 + \beta_d^2}}\right) \tag{1}$$

where LSi (i = 1~5) represents the ith damage limit state of structure; Φ(·) is the normal standard distribution function; $IDR_{\mathrm{LS}i}$ is the median interstorey drift ratio value of the i^{th} damage limit state; $\overline{IDR}_{\max}$ is the median value of the interstorey drift ratio response of the structures; β_c represents the logarithmic standard deviation of the $IDR_{\mathrm{LS}i}$; β_d represents the logarithmic standard deviation of the $IDR_{\max}$.

The calculation method of structural fragility curves for M-A sequences is the same as that of a single earthquake. The difference is that the structural demand for M-A sequences is larger, which is affected not only by the PGA of mainshock ($\mathrm{PGA}_{\mathrm{ms}}$), but also by the PGA of aftershock ($\mathrm{PGA}_{\mathrm{as}}$). Therefore, to calculate the fragility curves for M-A sequences, the $IDR_{\max}|\mathrm{PGA}$ will be replaced by $IDR_{\max}|\mathrm{PGA}_{\mathrm{seq}}$ for M-A sequences in Eq.(1). The $IDR_{\max}|\mathrm{PGA}_{\mathrm{seq}}$ represents the interstorey drift ratio for M-A sequences.

To facilitate statistical analysis, the relative intensity of aftershock (γ) is introduced and defined as the ratio of $\mathrm{PGA}_{\mathrm{as}}$ to $\mathrm{PGA}_{\mathrm{ms}}$. To investigate the influence of aftershocks with different intensity, 6 levels of γ is adopted: $\gamma = 0, 0.2, 0.4, 0.6, 0.8$, and 1.0, where $\gamma = 0$ considers only the mainshock effect.

3 Structural capacity and seismic demand assessment

3.1 Structural performance levels

Performance-based seismic design has been established over the last decades to set appropriate seismic performance objectives for structural design, so that the damage state and economic loss of the structure under severe earthquakes can meet the requirements of the owner/stakeholder. The performance level describes the structural damage limit state and the damage index required to define the damage limit state. According to the Reference [24][25], five performance levels are considered: (a) Negligible (LS1), (b) Minor (LS2), (c) Moderate (LS3), (d) Severe (LS4), and (f) Collapse (LS5), respectively. Common damage indices include the bearing capacity, deformation capacity, and energy consumption capacity. Investigations show [26][27] that storey displacement or interstorey drift ratio can comprehensively reflect the damage state of masonry structures, which is widely applied in seismic design and performance assessment.

There are great differences in the design of RC tie columns for masonry structures in different areas in China due to economical reasons, therefore, masonry wall systems are firstly classified to five classes according to the location of RC tie columns (see Fig.1), namely as: class A (no RC tie columns), class B (RC tie columns located at blue square in Fig.1), class C (RC tie columns located at blue and purple square in Fig.1), class D (RC tie columns located at blue, purple, and green square in Fig.1), and class E (RC tie columns located at blue, purple, green, and red square in Fig.1), respectively. For example, the masonry structures built in 1970s do not have structural columns, that is, class A in Fig. 1; The location of RC tie columns for masonry structures built in 2010s, which are located at all color squares, is same as class E in Fig. 1. Then, interstorey drift ratio limit values of each type of masonry structures are determined. Jiang et al. [28] summarized numerous investigations of brick wall tests and obtained the interstorey drift ratios corresponding to each performance level of masonry structures, as shown in Table 1. According to Borzi et al. [20], the interstorey drift ratio of each damage limit states obeys lognormal distribution. The coefficient of variations (COVs) of the interstorey drift ratios for LS1, LS2, LS3, LS4, and LS5 limit state are 35%, 30%, 35%, 35% and 35%, respectively. Finally, the maximum interstorey drift ratio due to M-A sequences was observed, and the degree of structural damage can be determined.

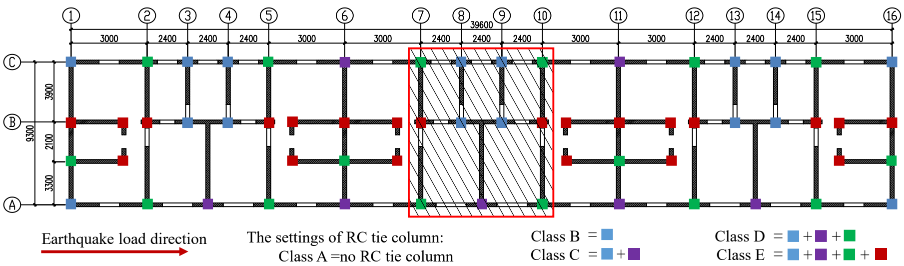

Fig. 1. Plane of basic structure model and the location of RC tie columns (unit: mm).

Table 1 Interstorey drift ratio limits for each performance level.

Performance level	Limit state	A	B	C	D	E
Negligible	LS1			0.04%		

Minor	LS2			0.08%		
Moderate	LS3			0.13%		
Severe	LS4	0.26%	0.28%	0.31%	0.39%	0.46%
Collapse	LS5	0.39%	0.43%	0.52%	0.65%	0.79%

3.2 Interstorey drift ratio demand

In this study, the failure mode of multi-storey masonry structures is assumed to be dominated by shear, and the storey shear capacity-storey displacement curve is assumed to follow the principles of the elastic-perfectly plastic (EPP) model. The storey yield strength coefficient ξ_i, can be calculated as Eq. (2) [29], is defined as the ratio of the ultimate shear strength of the i^{th} storey to the seismic shear force V_i of the i^{th} storey.

$$\xi_i = \frac{0.9R_{ui}}{V_i} = \frac{0.11\rho_i}{\alpha_{\max} g_e} \cdot \frac{n+1}{(n+i)(n-i+1)} \sqrt{f_{2,i} + \frac{8.33 g_e (n-i+1)\sqrt{f_{2,i}}}{\rho_i + \rho'_i}} \quad (2)$$

where ξ_i is the storey yield strength coefficient of the i^{th} storey; R_{ui} is the ultimate shear capacity of i^{th} storey; V_i is the seismic shear force of the i^{th} storey; g_e is a combined gravity load that consider the effect of dead load and live Load (1.0 Dead load + 0.5 Live Load) [24]; n is the number of storeys; $\alpha_{\max}$ is the maximum seismic influence coefficient, which can be determined as $\alpha_{\max}=2.25\cdot \mathrm{PGA}_{\mathrm{ms}}\cdot(1+0.03\cdot\gamma)$ for M-A sequences; ρ_i and ρ'_i is the seismic wall area ratio in calculation direction and orthogonal direction of the i^{th} storey, which represents the ratio of the cross-sectional area of masonry wall in half-storey height to the storey area; $f_{2,i}$ is average compressive strength of the mortar used in i^{th} storey. The coefficient of 0.11 in Eq. (2) should be changed to 0.11×0.85=0.094 [29] when n is equal to 1.

The strength reduction factor R can be expressed as the inverse of minimum ξ_i

(that is $\xi_{i,\min}$), which is shown in Eq. (3). Because RC tie column has a great influence on storey yield strength coefficient ξ_i (described in Fig. 2), influence coefficient η is introduced to consider the influence of RC tie columns on the lateral capacity of masonry structures. According to *Standard for seismic appraisal of buildings* [30], for class A, class B, class C, class D, and class E, the η are 1.0, 1.05, 1.1, 1.2, and 1.3 respectively.

$$R=\frac{1}{\eta\cdot\xi_{i,\min}}=\frac{\alpha_{\max}g_e n}{0.11\rho_i\sqrt{f_{2,i}+\dfrac{8.33ng_e\sqrt{f_{2,i}}}{\rho_i+\rho'_i}}} \tag{3}$$

Generally, the soft-storey of a regular masonry structure is located at the bottom storey of buildings, so the i in Eq.(3) can be approximated to be 1.

Considering the effect of shear deformation, bending deformation and coupling of wall limbs, Jiang et al. [31] proposed a calculation formula for the natural period $T_{0,e}$ of multi-storey masonry structures, which is expressed by Eq. (4).

$$T_{0,e}=\left(0.132+0.050\frac{H}{B}\right)\sqrt{\frac{g_e}{f_m^{1.5}h\rho}}\cdot H \tag{4}$$

where H and B are the structural height and width, respectively; f_m is the average compressive strength of masonry; h is the height of the soft-storey.

The ductility factor μ is obtained by R through R-μ-T relationship [32]. In this manuscript, the R-μ-T relationship proposed by Zhang [33], which is calculated as shown in Eq. (5), is adopted, because the expression considers the effect of M-A sequences.

$$R = 1 + \frac{a_0\left(a_1 T_{0,e} + T_{0,e}^2\right)\left(a_4 + \mu\right)}{\left(1 + a_2 T_{0,e} + a_3 T_{0,e}^2\right)\left(1 + a_5 \mu\right)} \frac{1}{0.87 + 0.08 e^{1.2\gamma}} \tag{5}$$

where a_0, a_1, a_2, a_3, a_4 and a_5 are parameters depending on site classes. The site classes are determined according to V_{20} [24] and listed in Table 2.

Table 2 The value of a_0~a_5.

Site class	V_{20}	V_{30}	a_0	a_1	a_2	a_3	a_4	a_5
I	$V_{20} > 500$m/s	$V_{30} > 596$m/s	0.86	10.83	9.68	0.57	-0.79	0.02
II	250m/s < $V_{20} \leq 500$m/s	278m/s < $V_{30} \leq 596$m/s	0.71	13.21	9.97	0.98	-0.84	0.01
III	150m/s < $V_{20} \leq 250$m/s	158m/s < $V_{30} \leq 278$m/s	1.03	10.93	11.49	0.77	-0.95	0.04
IV	$V_{20} \leq 150$m/s	$V_{30} \leq 158$m/s	0.66	13.25	9.95	0.55	-0.81	0.01

To evaluate the displacement response of masonry structures, an equivalent elastic single-degree-of-freedom system was proposed by Lin and Lin [34] is adopted, and the equivalent elastic period T_{eq} and the equivalent damping ζ_{eq} are computed by Eq. (6) and Eq. (7), respectively.

$$T_{eq} = T_{0,e}\sqrt{\mu} \tag{6}$$

$$\zeta_{eq} = \zeta_0 + 0.079 T_{0,e}^{-0.252}\sqrt{R-1} \tag{7}$$

where ζ_0 is the elastic viscous damping coefficient.

Based on T_{eq} and ζ_{eq}, the damping reduction factor B can be determined by Eq. (8) [29].

$$B = \begin{cases} 1 + \dfrac{0.05 - \zeta_{eq}}{0.06 + 1.4\zeta_{eq}} & (T_{eq} \leq T_g) \\ \left(1 + \dfrac{0.05 - \zeta_{eq}}{0.06 + 1.4\zeta_{eq}}\right) \cdot \left(\dfrac{T_g}{T_{eq}}\right)^{0.9 + \frac{0.05 - \zeta_{eq}}{0.5 + 5\zeta_{eq}}} & (T_{eq} > T_g) \end{cases} \tag{8}$$

where T_g is the characteristic period, which can be obtained from Reference [24].

The yield spectral displacement S_{dy} and inelastic spectral displacement S_{dp} can be obtained by Eq.(9) and Eq.(10) [35], respectively.

$$S_{dy} = \frac{S_{de}}{R} = \frac{T_{0,e}^2}{4\pi^2} \cdot \frac{\alpha_{\max} g}{R} \tag{9}$$

$$S_{dp} = \frac{T_{eq}^2}{4\pi^2} \cdot \alpha_{\max} g \cdot B \tag{10}$$

where S_{de} is the elastic spectral displacement of the single-degree-of-freedom (SDOF) system.

The inelastic displacement δ_p of the soft storey can be obtained by Eq.(11) [36].

$$\delta_p = \delta_y + \frac{S_{dp} - S_{dy}}{0.8 + 0.1n} = \frac{h}{\Gamma_h H} S_{dy} + \frac{S_{dp} - S_{dy}}{0.8 + 0.1n} \tag{11}$$

where δ_y is the yield displacement of the soft storey; Γ_h is the modal height coefficient.

The maximum interstorey drift ratio $IDR_{\max}$ can be estimated as Eq. (12).

$$IDR_{\max} = \delta_p / h \tag{12}$$

Base on the calculation of $IDR_{\max}$, the flow charts for the seismic fragility function of masonry structures is presented in Fig.2.

The proposed method (Eq. (2)~Eq. (11)) applies to the masonry structures with a height up to 21m, dominated by shear deformation, and with a uniform distribution of mass and stiffness along the height of the building. This method is not applicable to irregular structures with significant torsional effects. Moreover, the equivalent base shear method, which assumed that the horizontal seismic load is distributed in an inverted triangle along the height of the building, was adopted to establish Eq. (2) and Eq. (3).

The out-of-plane failure and the interaction between the in-plane and out-of-plane actions [37] is not considered in this study. When the vertical load of the masonry wall is small and the out-of-plane constraint is poor (e.g., wooden floor, large walls without out-of-plane support), the influence of out-of-plane damage should be considered, and further research is needed.

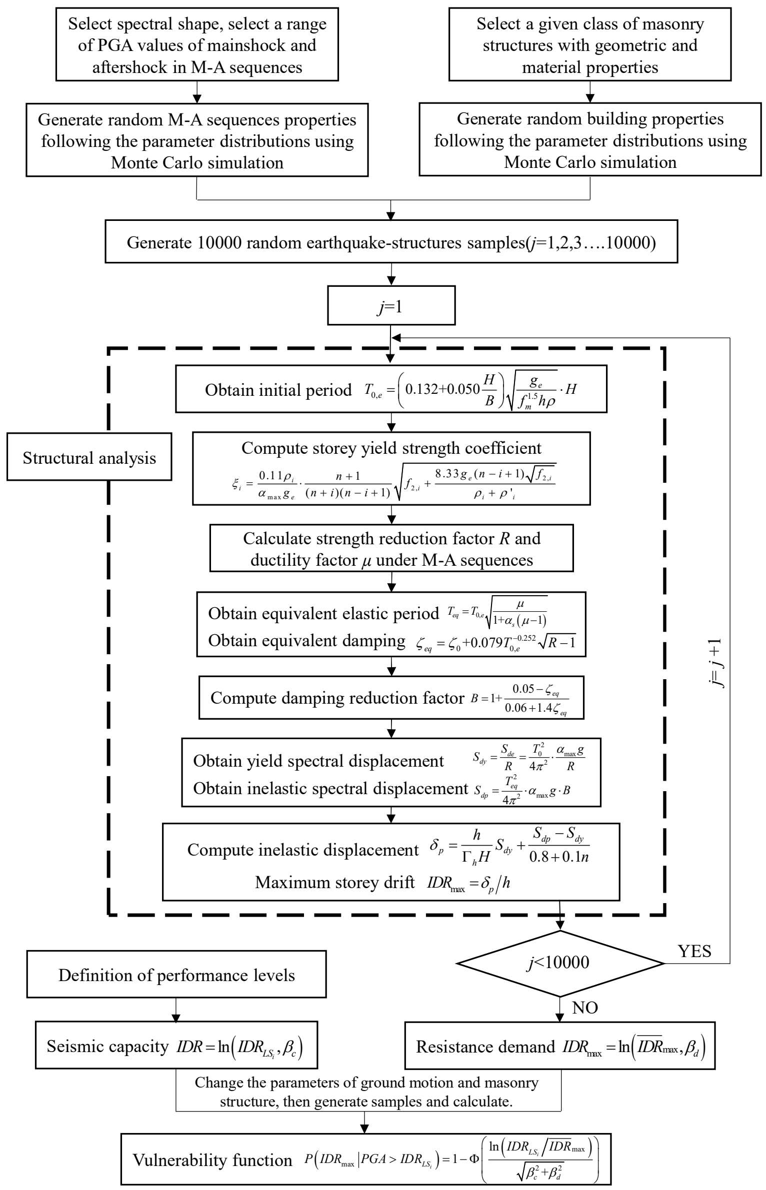

Fig. 2. Calculation flowchart of seismic fragility analysis of masonry structures.

The effect of hysteretic energy on structural damage is not considered in this method. The reason is that when the two-parameter model (e.g. Park-Ang model) is used as the damage index, the R-μ-T relationship of Eq. (5) will be replaced by the R-μ-D-T relationship [38][39], in which the D and μ are unknown and the calculation flowchart (see Fig. 2) cannot continue.

4 Earthquake-structure system

4.1 Basic structure model (BSM)

A 5-storey masonry structure was designed as the basic structure model (BSM), with a storey height of 3.0m, as shown in Fig. 1. The width and length of BSM is 9.3m and 39.6m, respectively. The thickness of all masonry walls is 240mm, so the ρ (X-direction) and ρ' (Y-direction) are 0.049 and 0.084, respectively. The g_e is 12.0kN/m^2. The compressive strength of mortar and masonry are 2.5MPa and 2.90MPa, respectively. The site condition of BSM is site class II.

4.2 Random variables to describe uncertainty in earthquake-structure system

The structural response is determined by the characteristics of structures and earthquakes. As a result, the uncertainty of an earthquake-structure system includes structural uncertainty and earthquake uncertainty. There are many factors causing the uncertainty of masonry structures, including the uncertainty of materials and the uncertainty of geometry dimensions. The compressive strength of mortar f_2 and masonry f_{m} are used as random variables to reflect the uncertainty induced by the construction of masonry walls. The length L, width B, height h, and wall thickness t of masonry structures are used as random variables to reflect the uncertainty induced by the geometrical dimensions of the structures themselves. Moreover, to comprehensively reflect the uncertainty of structures, it is also necessary to investigate the elastic damping ratio ξ, the seismic wall area ratio ρ, and the combined gravity load g_e. Moreover, the PGA_{ms} and characteristic period T_g are employed to reflect the uncertainty induced to the analysis system by the M-A sequences. The lower value of PGA_{ms} is 0. The curve of α_{max}, which is related to PGA of the input seismic motions, is plotted in Fig. 3 according to Chinese code GB 50011-2010 [24]. The characteristics of the parameter uncertainty of the BSM are shown in Table 3.

Table 3 Random variables used in basic structure model and earthquake motions.

Parameter	Mean Value	Coefficient of variation	Distribution model	references
Height h(m)	3.0	5.0%	Normal	[20], [21]
Length L(m)	39.6	5.0%	Normal	[20], [21]
Width B(m)	9.3	5.0%	Normal	[20], [21]
Wall thickness t(m)	0.24	5.0%	Normal	[20], [21]
Compression strength of masonry f_m(MPa)	2.90	17.0%	Normal	[20], [21], [40]
Compression strength mortar f_2(MPa)	2.5	30.0%	Normal	[20], [21], [40]
Seismic wall area ratio of Y-direction wall ρ'	0.084	3.5%	Normal	[20]

Seismic wall area ratio of X-direction wall ρ	0.049	4.1%	Normal	[20]
Combined gravity load g_e	11.0	7.0%	Normal	[40]
Elastic damping ratio ξ	0.05	30.0%	Normal	[40]
PGA of mainshock PGA_{ms}	—	44.0%	Lognormal	[20], [40]
Characteristic period T_g(s)	0.55	10.5%	Uniform	[20]

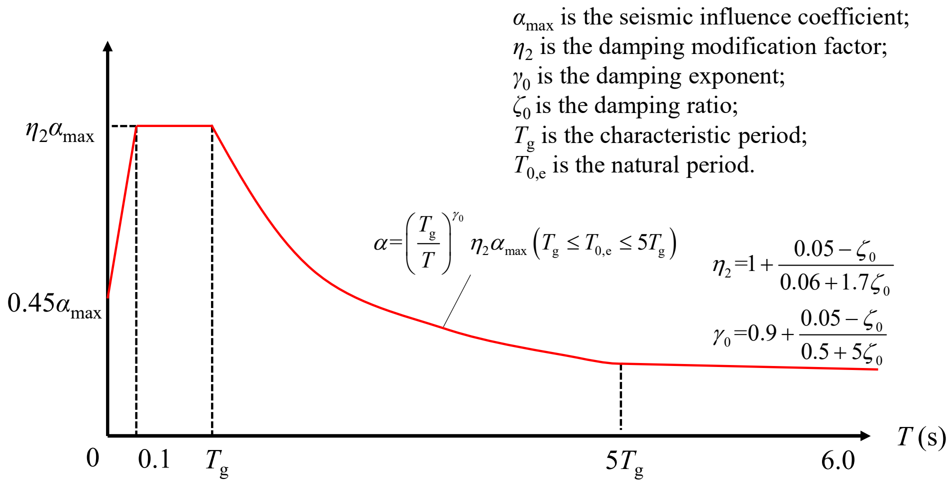

Fig. 3. Seismic influence coefficient curve specific in GB 50011-2010 [24].

4.3 Earthquake-structure samples

Monte Carlo simulations were employed to generate random variables of earthquake-structure system. To analyze the effect of different parameters on the fragility curves of masonry structures, a total of 3,600 structure models were developed, corresponding to the earthquake-structure system with 2 levels of seismic wall area ratio, 6 levels of aftershock intensity, 4 levels of site condition, 3 levels of number of storeys, 5 levels of the location of RC tie columns, and 5 levels of mortar strength. Each model generates 10,000 earthquake-structure samples, thus 36,000,000 earthquake-structure samples were obtained by developing 3,600 structure models.

5 Seismic fragility curves

According to the procedure described in Section 3, a total of 36,000,000 earthquake-structure samples are used to develop the seismic fragility curves. The fragility curves of masonry structures with different ρ is shown in Fig. 4, the X-axis represents PGA_{ms}, and the Y-axis represents the exceeding probability for different damage limit states.

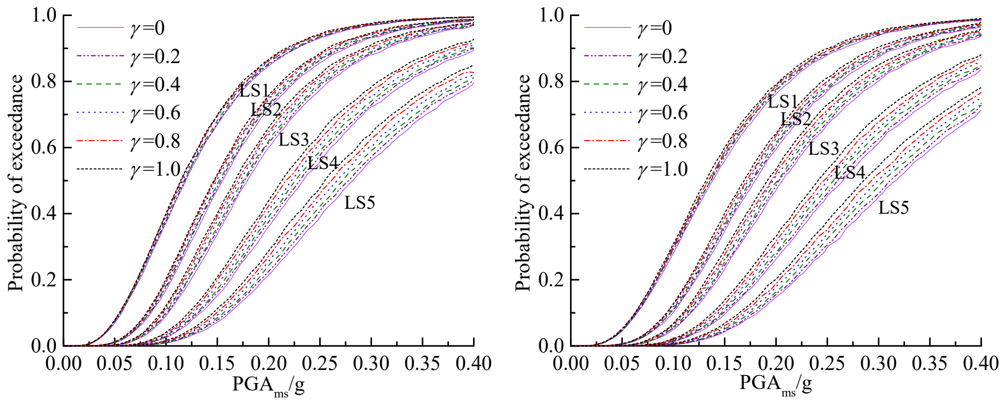

(a) Seismic wall area ratio ρ = 0.049 (b) Seismic wall area ratio ρ = 0.068

Fig. 4. The fragility curves for M-A sequences with different ρ and γ.

For the same damage limit state, the exceeding probability of masonry structures increases as PGA_{ms} increases. Namely, with the increment of the earthquake intensity, more masonry structures exceed the given damage limit state. Moreover, under same PGA_{ms}, as the damage state worsens, the exceeding probability of the structures gradually decreases.

The wall thickness of BSM is 240 mm, and ρ is 0.049. To study the influence of ρ, the thickness of exterior walls in BSM is changed to 370mm, and the corresponding ρ

is 0.068. As shown in Fig. 4, when PGA_{ms}=0.2g and γ=1.0, the exceeding probability of LS1 for ρ=0.049 and 0.068 are 86.6% and 79.1%, respectively. The exceeding probability of LS3 for ρ=0.049 and 0.068 are 66.0% and 53.4%, respectively. The exceeding probability of LS5 for ρ=0.049 and 0.068 are 28.7% and 20.2%, respectively. The results show that the greater the ρ, the lower the vulnerability of masonry structures. The earthquake load is mainly beared by the walls along the direction of earthquake load. Therefore, the greater the ρ, the better the seismic performance, and the lower the structural vulnerability.

When PGA_{ms}=0.2g and γ=0, 0.2, 0.4, 0.6, 0.8, and 1.0, the exceeding probability of LS1 for BSM (see Fig. 4a) are 85.2%, 85.3%, 85.6%, 85.9%, 86.2%, and 86.6%, respectively. The exceeding probability of LS3 for BSM are 60.0%, 61.4%, 62.1%, 63.8%, 64.7%, and 66.0%, respectively, while the exceeding probability of LS5 for BSM are 21.4%, 22.6%, 24.4%, 25.6%, 27.2%, and 28.7%, respectively. The results show that with the increment of the γ, M-A sequences induce higher levels of damage resulting in greater vulnerability of the system. When γ is less than 0.6, the difference of the exceeding probability between the mainshock analysis and M-A sequences analysis was found to be less than 10%, indicating that the aftershock effect can be ignored. When γ is greater than 0.6, the difference of the exceeding probability between the mainshock analysis and M-A sequences analysis was found to be greater than 10%, indicating that the aftershock effect should be considered in the preliminary design of the structures. The exceeding probability of LS5 for an aftershock with γ=1.0 is 32.2%

higher (in average) than that when the structure is subjected to a mainshock only.

5.1 Effect of site condition

To investigate the effect of site condition on fragility curves, four site condition of BSM are considered: site class I, site class II, site class III, and site class IV, respectively, remaining the other parameters of BSM unchanged. Fig. 5 shows the fragility curves of the BSM with different site condition.

For the masonry structures located at site class I, site class II, site class III, and site class IV, when PGA_{ms}=0.2g and γ=1.0, the exceeding probability of LS1 are 74.5%, 86.6%, 92.9%, and 89.2%, respectively; the exceeding probability of LS3 are 49.8%, 66.0%, 73.0%, and 69.9%, respectively; the exceeding probability of LS5 are 15.3%, 28.7%, 39.6%, and 33.7%, respectively. The results show that there are significant differences in the seismic fragility curves of masonry structures located at different site condition. The reason is that the characteristic periods T_g of each site class are different, among which the characteristic period of class I site is 0.2-0.35s, site class II is 0.35-0.45s, site class III is 0.45-0.65s, and class IV site is 0.65-0.90s. However, the initial period T_0 of the BSM is approximately 0.39s. According to *Code for seismic design of buildings* [24], the spectral acceleration of site class I is significantly smaller than that of other site classes, resulting in smaller vulnerability for the system. Due to the randomness of T_0 and T_g, the T_g of site class II might also be smaller than the T_0. As a result, the vulnerability of the system for site class II is smaller than that of site class III. For site class III and site class IV, the latter has a greater strength reduction factor than the former, so the effect of the latter is smaller than the former, thus system's vulnerability of the latter is smaller than the former.

For the masonry structures located at site class I, site class II, site class III, and site class IV, the exceeding probability of LS1 for γ=1.0 is 1.04, 1.01, 1.01, and 1.02 times of that for γ=0, respectively, while the exceeding probability of LS5 for γ=1.0 is 1.36, 1.23, 1.19, and 1.21 times of that for γ=0, respectively. The results show that the increase of the exceeding probability for site class II, III and IV is basically the same under the same γ, while the increase of the exceeding probability for site I was found to be larger, indicating that aftershocks have greater impact on masonry structures located at site class I.

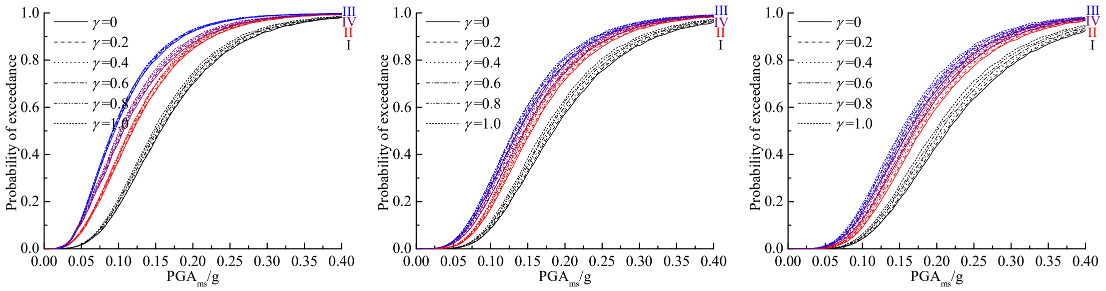

(a) LS1 (b) LS2 (c) LS3

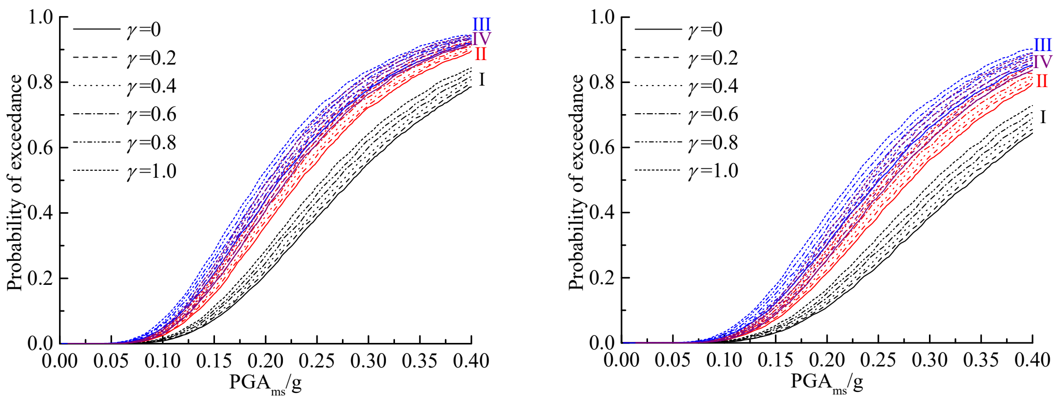

(d) LS4 (e) LS5

Fig. 5. The fragility curves of the masonry structures in different site classes.

5.2 Effect of number of storeys

To study the effect of the number of storeys n, the n is changed based on the BSM, and the n is set as 3, 4, and 5, respectively, the fragility curves for different n are are shown in Fig. 6.

As shown in Fig. 6, n has a significant impact on the seismic fragility curves of masonry structure. When PGA_{ms} is 0.2g and γ=1.0, the exceeding probability of LS1 for masonry structures with n = 3, 4, and 5 are 59.2%, 78.0%, and 86.6%, respectively. The exceeding probability of LS3 for structures with n = 3, 4, and 5 are 28.3%, 50.7%, and 66.0%, respectively. Accordingly, the exceeding probability of LS5 for structures with n = 3, 4, and 5 are 6.7%, 18.2%, and 28.7%, respectively. The results show that the exceeding probability increases significantly as n increases. Namely, the larger the n, the more severe the structural damage. As the n or total height increase, the overturning moment of the masonry structure increases, resulting in more severe damage to the structures induced by the greater base shear.

Earthquake damage investigation showed that the degree of structural damage in the same intensity zone is proportional to n. The larger the n, the higher the percentage of damage or collapse.

For masonry structures with n = 3, 4, and 5, the exceeding probability of LS1 for γ=1.0 is 1.04, 1.03, and 1.02 times of that for γ=0, while the exceeding probability of LS5 for γ=1.0 is 1.42, 1.33, and 1.24 times of that for γ=0. The results show that the effect of aftershocks increases with the decrease of the number of storeys.

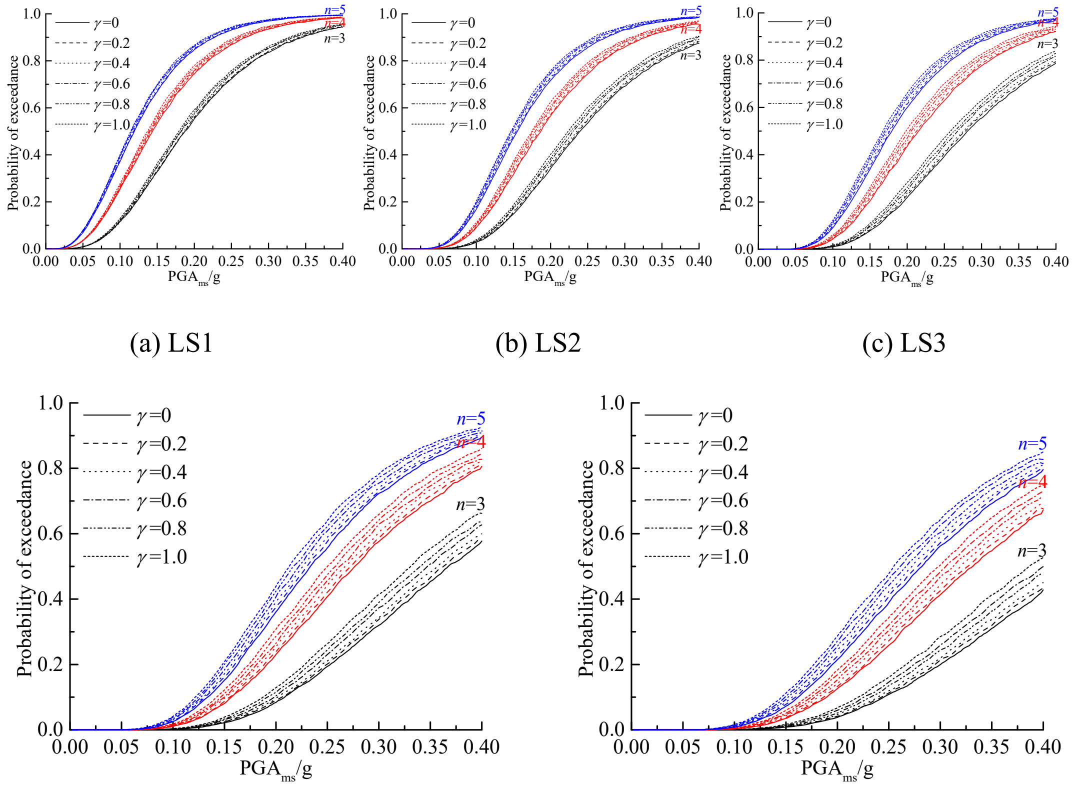

(a) LS1 (b) LS2 (c) LS3

(d) LS4 (e) LS5

Fig. 6. The fragility curves of masonry structures with different *n*.

5.3 Effect of RC tie column location

To investigate the effect of the location of RC tie columns, based on the BSM, five locations of RC tie columns, namely class A, class B, class C, class D and class E (see Fig.1), are adopted to calculate the fragility curves, as shown in Fig. 7.

For PGA_{ms} = 0.2g and γ =1.0, the exceeding probability of LS1 for class A, class B, class C, class D and class E are 86.6%, 85.6%, 84.0%, 81.8%, and 80.3%, respectively; the exceeding probability of LS3 for class A, class B, class C, class D and class E are 66.0%, 63.2%, 59.8%, 54.5%, and 49.1%, respectively. The difference of exceeding probability of LS1 for masonry structures with different location of RC tie columns is very small, which is also the same for the exceeding probability of LS2 and

LS3. The phenomenon indicates that the RC tie column has little influence on the structural performance before yielding. For PGA_{ms} =0.2g and γ=1.0, the exceeding probability of LS5 are 28.7%, 23.5%, 15.8%, 8.9%, and 4.9%, respectively. The exceeding probability of LS5 for masonry structures with different location of RC tie columns have a significant difference. The results show that reasonable setting of RC tie columns can reduce the exceeding probability of LS5 for 5-storey masonry structure from 28.7% to 4.9%, indicating that the RC tie column has a significant influence on the structural performance after yielding. The main reason is that RC tie column is effective at larger displacements to confine the masonry, thus improving the structural integrity and structural deformation capacity. Before yielding, the structural integrity is good, and the influence of RC tie column is small. After yielding, the RC tie column effectively ensures the structural integrity and improves the structural vulnerability, and the influence of RC tie column is significant. By increasing the number of RC tie columns in a masonry structure, the restraint of RC tie columns on masonry walls is stronger, the shear bearing capacity of the structure increases, displacements are reduced, and less damage is expected.

When the same damage limit for the interstorey drift ratio is adopted for masonry structures with different locations of RC tie columns, the damage state of masonry structure with class E will be overestimated while that of class A will be underestimated. As a result, for a given damage limit state, masonry structures with different locations of RC tie columns should adopt different limit values for the interstorey drift ratio, as shown in Table 1.

For the masonry structures with class A, class B, class C, class D and class E, the exceeding probability of LS1 for γ=1.0 is 1.01, 1.02, 1.02, 1.02, and 1.02 times of that for γ=0, respectively, while the exceeding probability of LS5 for γ=1.0 is 1.23, 1.28, 1.34, 1.44, and 1.54 times of that for γ=0, respectively. The results show that aftershocks have greater impact on the exceeding probability of LS4 and LS5 (see Fig. 7), indicating that aftershocks have a great influence on the masonry structure after yielding, but have small influence on the elastic region of the structural response. Moreover, the effect of aftershocks increases with the increase of the number of RC tie columns.

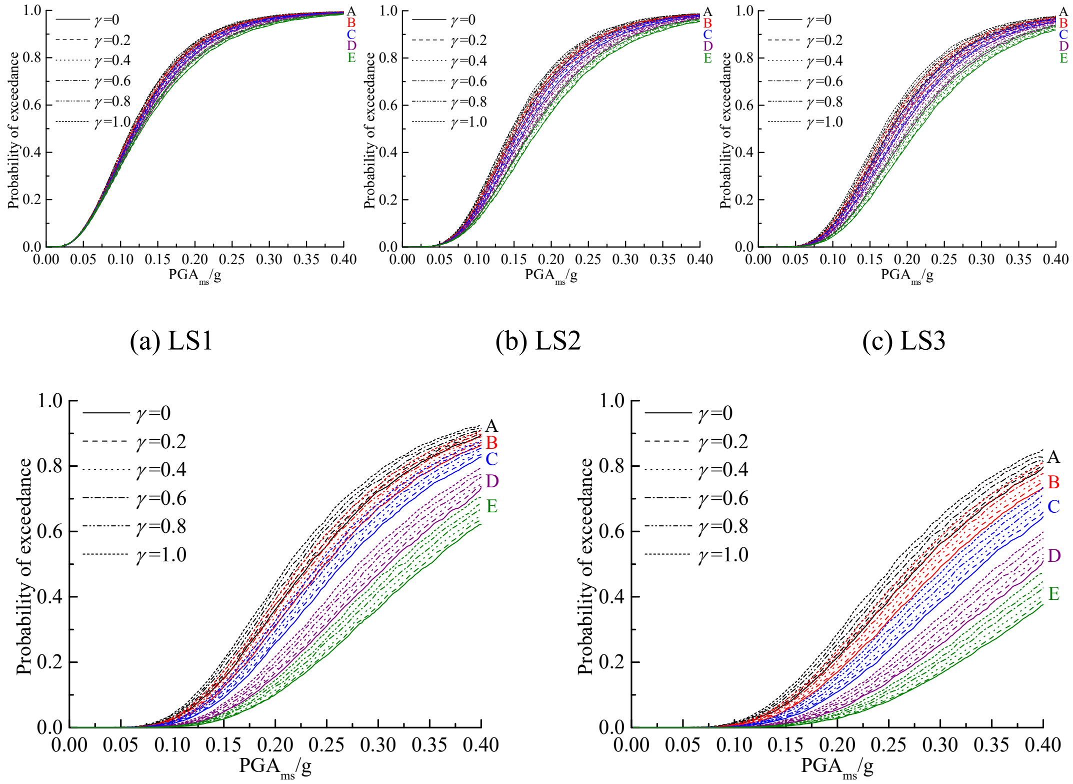

(a) LS1 (b) LS2 (c) LS3

(d) LS4 (e) LS5

Fig. 7. The curves of masonry structures with different setting of RC tie columns.

5.4 Effect of mortar strength

To study the effect of mortar strength f_2, based on the BSM, five mortar strengths, namely the f_2 = 1.0MPa, 2.5MPa, 5.0MPa, 7.5MPa and 10.0MPa, are adopted to calculate the seismic fragility curves, as shown in Fig. 8.

When PGA_{ms}=0.2g and γ=1.0, the exceeding probability of LS1 for masonry structures with f_2 = 1.0MPa, 2.5MPa, 5.0MPa, 7.5MPa and 10.0MPa are 94.7%, 86.6%, 75.3%, 64.2%, and 53.9%, respectively. The exceeding probability of LS3 for masonry structures with f_2 = 1.0MPa, 2.5MPa, 5.0MPa, 7.5MPa and 10.0MPa are 82.9%, 66.0%, 47.6%, 34.8%, and 25.3%, respectively. The exceeding probability of LS5 for masonry structures with f_2 = 1.0MPa, 2.5MPa, 5.0MPa, 7.5MPa and 10.0MPa are 44.8%, 28.7%, 17.2%, 11.0%, and 7.2%, respectively. The results show that as the f_2 increases, the structural performance increases significantly, and the vulnerability of the system gradually decreases. The shear strength of masonry increases with the increase of f_2, and the seismic capacity of the structures is improved. As a result, the stronger the mortar strength the lower the probability of exceeding a certain damage state.

For the masonry structures with f_2 = 1.0MPa, 2.5MPa, 5.0MPa, 7.5MPa and 10.0MPa, the exceeding probability of LS1 for γ=1.0 is 1.01, 1.01, 1.03, 1.04, and 1.05 times of that for γ=0, respectively, while the exceeding probability of LS5 for γ=1.0 is 1.19, 1.24, 1.31, 1.38, and 1.47 times of that for γ=0. The results show that the effect of the aftershocks increases with the increase of the f_2, respectively.

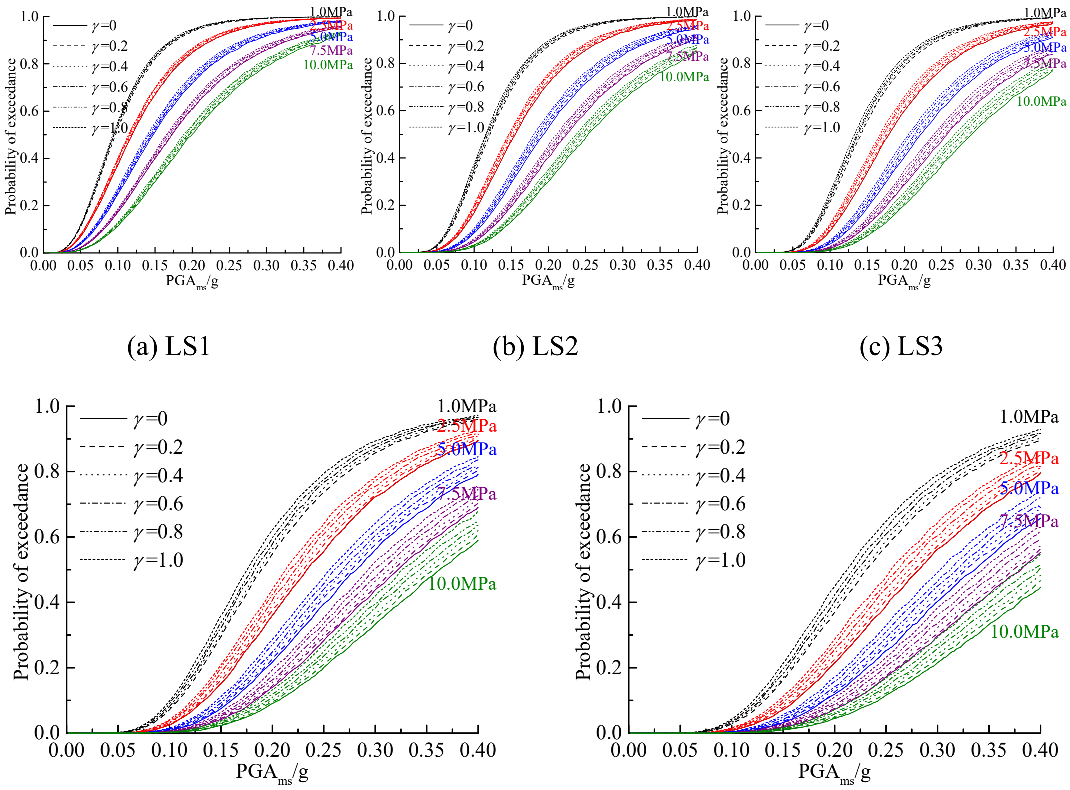

(a) LS1 (b) LS2 (c) LS3

(d) LS4 (e) LS5

Fig. 8. The fragility curves of masonry structures with different f_2.

5.5 Validation

5.5.1 Comparison between shake table tests and the proposed method

A part of the BSM was modeled (the shaded part of the masonry structure shown in Fig. 1) to verify the proposed approach for *IDR* demand of masonry structures. The shake table tests [41] were adopted to obtain *IDR* of the 1/4-scaled model, and the calculated results are compared with those calculated by the proposed method, as shown in Table 4. The measured natural period of the 1/4-scaled model is 0.126s and the similarity coefficient is 3.162:1, so the natural period of the BSM is 0.397s. The calculated natural period is 0.412s, and the error of the natural period is 3.8%, indicating that the calculated and experimental results have good consistency for the dynamic properties of the building structure. When the input PGA_{ms} = 0.035g, 0.10g, and 0.22g for mainshock only, the errors of IDR_{max} between calculated and average experimental results are all within 10.0%, indicating that the proposed method is reasonable.

Table 4 Validation of IDR_{max} of masonry structures.

	Experimental results		Numerical results		Calculated results
	El Centro	Taft	El Centro	Taft	
0.035g	1/2941	1/3393	1/2959	1/3217	1/3030
0.10g	1/1167	1/789	1/1214	1/744	1/857
0.22g	1/142	1/158	1/153	1/171	1/153

5.5.2 Comparison with fragility curves obtained from finite element method

Considering that fragility curves under M-A sequences are not available [42], the more accurate macro-modeling finite element method (FEM) which has been previously validated by the authors using shake table tests is adopted in this section to obtain the fragility curves of the 5-storey BSM (the shaded part of the masonry structure shown in Fig. 1). The natural periods of experimental and FEM results are 0.397s and 0.405s, and the error is 2.0%. It can be seen from Table 4 that the errors of *IDR* between experimental and FEM results are all within 10%. Then, the numerical results are compared with those obtained from the proposed calculation method. In macro-modeling finite element method, multilayer shell elements are used to simulate the masonry walls and reinforced concrete floors, as shown in Fig. 9. The macro-modeling method simplifies the brick and mortar into a homogenous material, the mechanical properties of which have been determined by both the brick and mortar. The plasticity model is employed to consider the constitutive laws of masonry and concrete, while the kinematic hardening model is used as the constitutive law of steel. The measured average compressive strength of masonry and mortar are 3.3MPa and 1.5MPa, respectively. The specific value of other material strengths can be referred to [41]. The failure of the element is determined by the maximum strain and stress rather than cumulative damage. To consider the uncertainty of ground motions, 8 M-A sequences, which are recorded from site class II, are selected from 8 earthquake events and used for the time history dynamic analysis. The specific finite element model and M-A sequence records can be found elsewhere [29]. Then, the interstorey drift ratios of the 5-storey BSM are calculated using dynamic time history analysis. Finally, the seismic fragility curves are obtained by adopting the incremental dynamic analysis method. The fragility curves of the BSM calculated by the above two methods subjected to M-A sequences with γ=0 and γ=1.0 are shown in Fig. 10. As expected, a good agreement can be observed between the seismic fragility curves obtained by the finite element method and the proposed method, which preliminary shows the feasibility of the proposed method. It should be noted that the dynamic time history analysis method takes nearly a week to completion, while the proposed method takes only 2 hours.

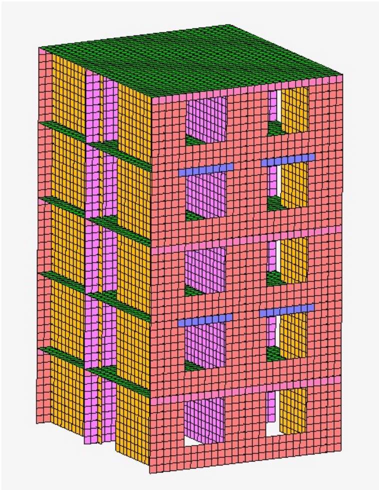

Fig. 9. The finite element model.

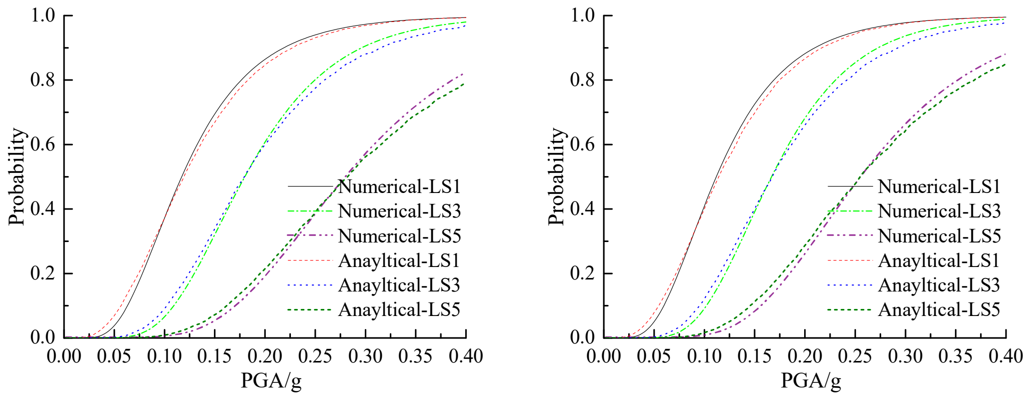

(a) γ=0 (b) γ=1.0

Fig. 10. Comparison between the fragility curves calculated by the finite element method and the proposed method in this manuscript.

5.6 Recommendation and Discussions

According to the analysis of the obtained fragility curves, the number of storeys has the greatest effect on the fragility of masonry structures, followed by the location and number of RC tie columns. The seismic wall area ratio and mortar strength follow, while it was found that the site conditions have the lowest impact. Since the geometric dimensions and the number of storeys has been pre-defined by the architects before structural analysis, the most effective way to improve the seismic performance of masonry structures is by placing a sufficient number of RC tie columns in original design. Using mortars with high strength is an alternative way to improve seismic performance. The effect of aftershock should be considered in the preliminary design of the structures when γ is less than 0.6.

6 Conclusion

This manuscript focuses on a simplified probabilistic approach for seismic fragility analysis of masonry structures considering the influence of aftershocks. 36,000,000 stochastic earthquake-structure system samples were generated by Monte Carlo simulation to calculate seismic fragility curves. The effect of aftershock intensity, seismic wall area ratio, site condition, number of storeys, RC tie column, and mortar strength were studied. The following conclusions can be drawn:

(1) Based on the characteristics of the soft storey mechanism of masonry structures, a simplified probabilistic approach for seismic fragility analysis of masonry structures under M-A sequences is proposed. The uncertainty of masonry structures and the uncertainty of earthquake ground motions are considered in the proposed method to generate a large database of earthquake-structure samples. Compared with the finite element methods, the proposed method can save computational time significantly while maintaining accuracy.

(2) Strong aftershocks can further aggravate the damage state of masonry structures. As the relative intensity γ of aftershock increases, structural vulnerability increases gradually. The effect of aftershock on structural performance can be ignored

when γ is less than 0.6. The probability of exceeding the collapse limit state of structures can increase by 32.2% when γ is equal to 1.0 (i.e., aftershock having equal intensity with the mainshock).

(3) The number of storeys n has the greatest influence on the seismic vulnerability of masonry structures. It was found that the exceeding probability of collapse damage state increases from 6.7% to 28.7% with the increases of n.

(4) RC tie columns can enhance the seismic performance of masonry structures, especially after yielding. By increasing the number of RC tie columns and selecting properly their location across the floor plan of the structure, the exceeding probability of collapse damage state decreases from 28.7% to 4.9%.

(5) The seismic wall area ratio ρ and the mortar strength f_2 strongly affects the seismic vulnerability of masonry structures. With the ρ increasing from 0.049 to 0.068, the exceeding probability of collapse damage state decreases from 28.7% to 20.2%. With the f_2 increasing from 1.0MPa to 10.0MPa, the exceeding probability of collapse damage state decreases from 44.8% to 7.2%.

CRediT authorship contribution statement

Yongqun Zhang: Conceptualization, Methodology, Investigation, Writing - original draft, Funding acquisition. **Zhuolin Wang:** Investigation, Formal analysis, Writing - original draft. **Lixue Jiang:** Supervision, Writing - review & editing. **Konstantinos Skalomenos:** Supervision, Writing - review & editing. **Dongbo Zhang:**

Validation, Writing - original draft.

Declaration of Competing Interest

None.

Acknowledgements

The authors would like to acknowledge the financial support provided by Scientific Research Fund of Institute of Engineering Mechanics, China Earthquake Administration (Grant No.2021D30), Natural Science Foundation of Shanghai (Grant No.21ZR1455000) and Shanghai Science and Technology Commission Program (Grant No. 19DZ1202400).

References

[1] Shin T C, Teng T. An Overview of the 1999 Chi-Chi, Taiwan, Earthquake. Bull Seismol Soc Am 2001; 91(5): 895-913.

[2] Wang Z. A preliminary report on the Great Wenchuan Earthquake. Earthq Eng Eng Vib 2008; 7(2): 225-34.

[3] Moon L, Dizhur D, Senaldi I, Derakhan H, Griffith M, Magenes G, Ingham J. The Demise of the URM Building Stock in Christchurch during the 2010-2011 Canterbury Earthquake Sequence. Earthq Spectra 2014; 30(1): 253-76.

[4] Kazama M, Noda T. Damage statistics (Summary of the 2011 off the Pacific Coast

of Tohoku Earthquake damage). Soils Found 2012; 52(5): 780-92.

[5] Chen H, Xie Q, Li Z, Xue W, Liu K. Seismic Damage to Structures in the 2015 Nepal Earthquake Sequences. J Earthq Eng 2017; 21(4): 551-78.

[6] Wen W, Zhai C, D Ji, Li S, Xie L. Framework for the vulnerability assessment of structure under mainshock-aftershock sequences. Soil Dyn Earthq Eng 2017; 101: 41-52.

[7] Abdelnaby A E. Fragility curves for RC frames subjected to Tohoku mainshock aftershocks sequences. J Earthq Eng 2018; 22(5): 902-20.

[8] Panchireddi B, Ghosh J. Cumulative vulnerability assessment of highway bridges considering corrosion deterioration and repeated earthquake events. Bull Earthq Eng 2019; 17(3): 1603-38.

[9] Li X, Wen W, Zhai C. A probabilistic framework for the economic loss estimation of structures considering multiple aftershocks. Soil Dyn Earthq Eng 2020; 133: 106121.

[10] Di Sarno L, Pugliese F. Seismic fragility of existing RC buildings with corroded bars under earthquake sequences. Soil Dyn Earthq Eng 2020; 134: 106169.

[11] Li Q, Ellingwood B R. Performance evaluation and damage assessment of steel frame buildings under main shock-aftershock earthquake sequences. Earthq Eng Struct Dyn 2007; 36(3): 405-27.

[12] Ruiz-García J, Negrete-Manriquez J C. Evaluation of drift demands in existing steel frames under as-recorded far-field and near-fault mainshock-aftershock

seismic sequences. Eng Struct 2011; 33(2): 621-34.

[13] Di Sarno L, Wu J R. Fragility assessment of existing low-rise steel moment-resisting frames with masonry infills under mainshock-aftershock earthquake sequences. Bull Earthq Eng 2021; 19(6): 2483-504.

[14] Goda K, Salami M R. Inelastic seismic demand estimation of wood-frame houses subjected to mainshock-aftershock sequences. Bull Earthq Eng 2014; 12(2): 855-74.

[15] Zhang L, Goda K, De Luca F, De Risi R. Mainshock-aftershock state-dependent fragility curves: A case of wood-frame houses in British Columbia, Canada. Earthq Eng Struct Dyn 2020; 49(9): 884-903.

[16] Rinaldin G, Amadio C. Effects of seismic sequences on masonry structures. Eng Struct 2018; 166: 227-39.

[17] Zhao B, Taucer F, Rossetto T. Field Investigation on the Performance of Building Structures during the 12 May 2008 Wenchuan Earthquake in China. Eng Struct 2009; 31(8):1707-23.

[18] Sun B, Zhang G. Study on vulnerability matrices of masonry buildings of mainland of China. Earthq Eng Eng Vib 2018; 17(2): 251-59.

[19] Asteris P G, Chronopoulos M P, Chrysostomou C Z, Varum H, Plevris V, Kyriakides N, Silva V. Seismic vulnerability assessment of historical masonry structural systems. Eng Struct 2014; 62-63: 118-34.

[20] Borzi B, Crowley H, Pinho R. Simplified pushover-based earthquake loss

assessment (SP-BELTA) method for masonry buildings. Int J Archit Herit 2008; 2(4): 353-76.

[21] Ahmad N, Ali Q. Displacement based seismic assessment of masonry buildings for global and local failure mechanisms. Cogent Eng 2017; 4(1): 1414576.

[22] Lagomarsino S, Cattari S, Ottonelli D. The heuristic vulnerability model: fragility curves for masonry buildings. Bull Earthq Eng 2021; 19(8): 3129-63.

[23] Shabani A, Kioumarsi M, Zucconi M. State of the art of simplified analytical methods for seismic vulnerability assessment of unreinforced masonry buildings. Eng Struct 2021; 239: 112280.

[24] GB50011-2010. Code for seismic design of buildings. Beijing, China: China Architecture and Building Press; 2010. [in Chinese]

[25] Zhang Y, Jiang L, Wang Z. Simplified displacement-based earthquake loss assessment method for masonry structures. In: The 17th World Conference of Earthquake Engineering, Sendai, Japan; 2020.

[26] Acevedo A B, Jaramillo J D, Yepes C, Silva V, Osorio F A, Villar M. Evaluation of the seismic risk of the unreinforced masonry building stock in Antioquia, Colombia. Nat Hazards 2017; 86(1): 31-54.

[27] Lagomarsino S, Giovinazzi S (2006) Macroseismic and mechanical models for the vulnerability and damage assessment of current buildings. Bull Earthq Eng 2006; 4(4): 415-43.

[28] Jiang L, Wang Z, Zhang F. Damage degree and inter-story drift angle limit of multi-

story masonry structures. J Build Struct 2018; 39(S2): 263-70. (in Chinese)

[29] Zhang Y, Wang Z, Jiang L, Skalomenos K, Zhang D. Seismic analysis method of unreinforced masonry structures subjected to mainshock-aftershock sequences. Bull Earthq Eng 2022; 20(5): 2619-41.

[30] GB 50023-2009. Standard for seismic appraisal of buildings. Beijing, China: Architecture and Building Press; 2009. (in Chinese)

[31] Jiang L, Wang Z, Jiang L. Approximate calculation method for fundamental period of multi-story masonry structures. J Build Struct 2018; 39(S2): 254-62.

[32] Elnashai A S, Di Sarno L. Fundamentals of earthquake engineering (2nd Edition). Chichester (UK): Wiley & Sons; 2015.

[33] Zhang Y. Ductility-based strength reduction factor for mainshock-aftershock sequence-type ground motions. Build Struct 2020; 50(14): 97-103. [in Chinese]

[34] Lin Y, Lin Y. Non-iterative equivalent linearization based on secant period for estimating maximum deformations of existing structures. J Earthq Eng 2009; 13(2): 170-92.

[35] Fajfar P. Capacity spectrum method based on inelastic demand spectra. Earthq Eng Struct Dyn 1999; 28(9): 979-93.

[36] Restrepo-Velez L F. A simplified mechanics-based procedure for the seismic risk assessment of unreinforced masonry buildings. Individual Study. Pavia, Italy: ROSE School; 2003.

[37] Mazza F, Donnici A. In-plane and out-of-plane seismic damage of masonry infills

in existing r.c. structures: the case study of De Gasperi-Battaglia school in Norcia. Bull Earthquake Eng 2021; 19(1): 345-76.

[38] Zhang Y, Shen J, Chen J. Damage-based yield point spectra for sequence-type ground motions. Bull Earthq Eng 2020; 18(10): 4705-24.

[39] Zhang Y, Chen J, Sun C. Damage-based strength reduction factor for nonlinear structures subjected to sequence-type ground motions. Soil Dyn Earthq Eng 2017; 92(1): 298-311.

[40] Zhai X M, Stewart M G. Structural reliability analysis of reinforced grouted concrete block masonry walls in compression. Eng Struct 2010; 32(1): 106-14.

[41] Chen X, Zhang Y, Wang Z, Yu J, Skalomenos K, Xu Q. Shaking table tests on a 5-storey unreinforced masonry structure strengthened by ultra-high ductile cementitious composites. J Build Eng 2022; 54: 104635.

[42] Lovon H, Tarque N, Silva V, Yepes-Estrada C. Development of Fragility Curves for Confined Masonry Buildings in Lima, Peru. Earthq Spectra 2018; 34(3): 1339-61.